termis.

Tissue Engineering
& Regenerative Medicine
International Society

ORIGINAL ARTICLE

Competitive Protein Binding Influences Heparin-Based Modulation of Spatial Growth Factor Delivery for Bone Regeneration

Marian H. Hettiaratchi, PhD,[1] Catherine Chou,[1] Nicholas Servies, BS,[1] Johanna M. Smeekens, BS,[2] Albert Cheng, MS,[3,4] Camden Esancy, BS,[3] Ronghu Wu, PhD,[2,3] Todd C. McDevitt, PhD,[5,6] Robert E. Guldberg, PhD,[3,4] and Laxminarayanan Krishnan, MBBS, PhD[3]

Tissue engineering strategies involving the *in vivo* delivery of recombinant growth factors are often limited by the inability of biomaterials to spatially control diffusion of the delivered protein within the site of interest. The poor spatiotemporal control provided by porous collagen sponges, which are used for the clinical delivery of bone morphogenetic protein-2 (BMP-2) for bone regeneration, has necessitated the use of supraphysiological protein doses, leading to inflammation and heterotopic ossification. This study describes a novel tissue engineering strategy to spatially control rapid BMP-2 diffusion from collagen sponges *in vivo* by creating a high-affinity BMP-2 sink around the collagen sponge. We designed an electrospun poly-ε-caprolactone nanofiber mesh containing physically entrapped heparin microparticles, which have been previously demonstrated to bind and retain large amounts of BMP-2. Nanofiber meshes containing 0.05 and 0.10 mg of microparticles/cm² demonstrated increased BMP-2 binding and decreased BMP-2 release *in vitro* compared with meshes without microparticles. However, when microparticle-containing meshes were used *in vivo* to limit the diffusion of BMP-2 delivered by using collagen sponges in a rat femoral defect, no differences in heterotopic ossification or biomechanical properties were observed. Further investigation revealed that, although BMP-2 binding to heparin microparticles was rapid, the presence of serum components attenuated microparticle-BMP-2 binding and increased BMP-2 release *in vitro*. These observations provide a plausible explanation for the results observed *in vivo* and suggest that competitive protein binding *in vivo* may hinder the ability of affinity-based biomaterials to modulate growth factor delivery.

Keywords: bone morphogenetic protein, collagen sponge, heparin microparticles, heterotopic ossification, nanofiber mesh, spatial control of bone regeneration

Introduction

MUSCULOSKELETAL INJURIES RESULTING in significant bone loss affect millions of people each year. In the United States alone, ~1 million fractures requiring additional intervention occur each year.[1] The delivery of recombinant growth factors can stimulate cell recruitment and endogenous repair mechanisms to heal injured bone and presents a promising strategy for the treatment of large bone defects.[2–5] Several successful clinical trials for anterior lumbar spinal fusions, open tibial fractures, and sinus augmentations have been completed by using recombinant human bone morphogenetic protein-2 (rhBMP-2) and have demonstrated comparable efficacy to bone grafts, leading to FDA approval of rhBMP-2 delivery for these three specific applications.[6–10] However, promising clinical outcomes have also led to the widespread ''off-label'' use of BMP-2 for other bone regeneration applications,[11] including posterior and transforaminal lumbar fusions.[12] In addition to reducing the efficacy of BMP-2 in forming orthotopic bone,

[1]The Wallace H. Coulter Department of Biomedical Engineering, Georgia Institute of Technology and Emory University, Atlanta, Georgia.
[2]School of Chemistry and Biochemistry, Georgia Institute of Technology, Atlanta, Georgia.
[3]The Parker H. Petit Institute for Bioengineering and Bioscience, Georgia Institute of Technology, Atlanta, Georgia.
[4]The George W. Woodruff School of Mechanical Engineering, Georgia Institute of Technology, Atlanta, Georgia.
[5]The Gladstone Institute of Cardiovascular Disease, San Francisco, California.
[6]The Department of Bioengineering and Therapeutic Sciences, University of California San Francisco, San Francisco, California.

rapid diffusion of high doses of BMP-2 away from the tissue injury site can cause excessive soft tissue inflammation[13,14] and heterotopic ossification adjacent to the implant site[11,15] in 23–28% of patients treated with BMP-2 for off-label spinal fusion procedures.[13,14]

The collagen sponge, commonly used in surgeries as a BMP-2 delivery vehicle, entraps BMP-2 through weak electrostatic interactions, resulting in a burst release of BMP-2 on implantation in the tissue defect.[16–19] The lack of definitive dose–response data for BMP-2 delivery may have contributed to the use of supraphysiological rhBMP-2 doses (≥0.2 mg/kg body weight) clinically,[20] to ensure that a sufficient dose of bioactive BMP-2 remains at the site of interest. The incidence of adverse events after BMP-2 treatment has also been correlated with an increased BMP-2 dose.[12] Collagen sponge delivery of 150–2500 µg of BMP-2 in a canine spinal fusion model resulted in improved mineralization at lower doses and the occurrence of large heterotopic bone cysts at higher doses.[21] BMP-2 delivery in a rat femoral defect model using an apatite-coated poly(lactic-co-glycolic) acid (PLGA) scaffold revealed that a lower BMP-2 dose (2.25 µg) induced bony bridging over 8 weeks, but higher BMP-2 doses (11.25–45 µg) resulted in the formation of abnormal bone and soft tissue swelling.[22] In our model of a rat femoral bone defect, we have similarly demonstrated the formation of heterotopic bone by using a 30 µg dose of BMP-2.[23]

Since the collagen sponge lacks specific affinity for BMP-2, biomaterials that strongly bind BMP-2 may provide better spatiotemporal control of its delivery and reduce the incidence of adverse events. Sulfated glycosaminoglycans (GAGs), such as heparin, heparan sulfate, and chondroitin sulfate, possess a strong affinity for BMP-2 and can electrostatically bind specific positively charged domains on BMP-2 through negatively charged sulfate groups on their linear polysaccharide structures.[24–26] Heparin, in particular, demonstrates strong BMP-2 binding ($K_D = 20$ nM)[27] and has been successfully integrated into a variety of tissue engineering scaffolds to improve BMP-2 retention and potency *in vivo*.[28–34] We have previously fabricated heparin-based microparticles that can be dose dependently incorporated into tissue engineering scaffolds. The high heparin density of these microparticles allows for the binding of >1000 times the amount of bioactive BMP-2 previously documented for other heparin-containing materials and retention of >80% of the bound growth factor over a period of 4 weeks *in vitro*.[35]

Here, we present a novel strategy of physically entrapping heparin microparticles (MP) within a poly-ε-caprolactone (PCL) nanofiber mesh tube to create a barrier to rapid BMP-2 diffusion from the clinical collagen sponge. This design allows clinicians the choice of current delivery methods, thus lowering adoption barriers. The distribution of microparticles deposited in the nanofiber meshes was assessed at two densities (0.05 and 0.10 mg MP/cm^2), followed by an *in vitro* evaluation of BMP-2 binding and release. The hybrid mesh was evaluated *in vivo* in a critically sized rat femoral defect model by using a supraphysiological dose of BMP-2 (30 µg) delivered within a collagen sponge; remineralization of the defect space and the extent of heterotopic ossification were evaluated. We hypothesized that heparin microparticles incorporated into the PCL mesh tube

would act as a growth factor sink, by binding BMP-2 released from the collagen sponge after implantation and limiting the exposure of surrounding tissues to high BMP-2 doses, thereby reducing heterotopic ossification while promoting effective bone repair.

Materials and Methods

Heparin microparticle fabrication

Heparin microparticles were fabricated from modified heparin methacrylamide[36] as previously described.[35] Briefly, heparin methacrylamide was combined with ammonium persulfate (APS; Sigma-Aldrich) and tetramethylethylenediamine (TEMED; Sigma-Aldrich) in phosphate-buffered saline (PBS; Corning Mediatech, Manassas, VA) and homogenized into 60 mL of corn oil. The water-in-oil emulsion was then heated to 55°C for 30 min under nitrogen purging to activate free radical cross-linking of the methacrylamide groups. Microparticles were centrifuged and retrieved after several acetone and ddH$_2$O washes, disinfected by rinsing in 70% ethanol solution for 30 min, and lyophilized for 24 h before use.

Fabrication of electrospun PCL nanofiber meshes

A 12% (w/v) solution of PCL (Sigma-Aldrich) in 90:10 hexafluoro-2-propanol (HFP; Sigma-Aldrich) and dimethylformamide (DMF; Sigma-Aldrich) was loaded into a syringe (Becton Dickinson, Franklin Lakes, NJ) with a 0.64 mm-diameter blunt tip needle (Howard Electronic Instruments, El Dorado, KS), and it was mounted onto a PHD2000 infusion syringe pump (Harvard Apparatus, Holliston, MA) that was set to an infusion rate of 0.75 mL/h. The electrospinning setup was assembled as previously described,[37] and a rectangular copper collection plate covered with aluminum foil was used for PCL nanofiber deposition. Then, 3.6 mL of PCL solution was infused through the syringe pump, creating a circular nanofiber mesh with an area of ∼100 cm^2 and a thickness of ∼500 µm. Meshes were desiccated to remove additional organic solvent.

Heparin microparticles were sprayed onto the meshes, after 1.2 and 2.4 mL of PCL had been electrospun (Fig. 1A), and physically entrapped within the meshes. 2.5 or 5 mg of microparticles suspended in ethanol was sprayed evenly across the mesh by using an airbrush (Iwata Medea, Inc., Portland, OR) that was driven by an air pump (TCP Global Co., San Diego, CA). Spraying each suspension twice entrapped microparticles in two layers between polymer fibers and created 0.05 and 0.10 mg MP/cm^2 meshes. In a similar manner, 0.05 mg MP/cm^2 meshes containing 4 µm diameter polystyrene microparticles (Polysciences, Inc., Warrington, PA) were also fabricated as an uncharged microparticle control. Meshes without microparticles received two empty ethanol sprays after 1.2 and 2.4 mL of PCL had been electrospun. Next, 12 mm by 19 mm sheets of electrospun PCL with or without twenty-three 0.9 mm-diameter perforations were laser cut from the meshes (Universal Laser Systems, Scottsdale, AZ), rolled into tubes (diameter 5 mm, length of 12 mm), and glued by using ultraviolet (UV) cure adhesive (1187-M MD Medical Device Adhesives and Coatings, BlueWave LED Prime UVA Spot Curing System; DYMAX, Torrington, CT). The length of the mesh tubes (12 mm) ensured sufficient overlap with the bone ends of the defect space
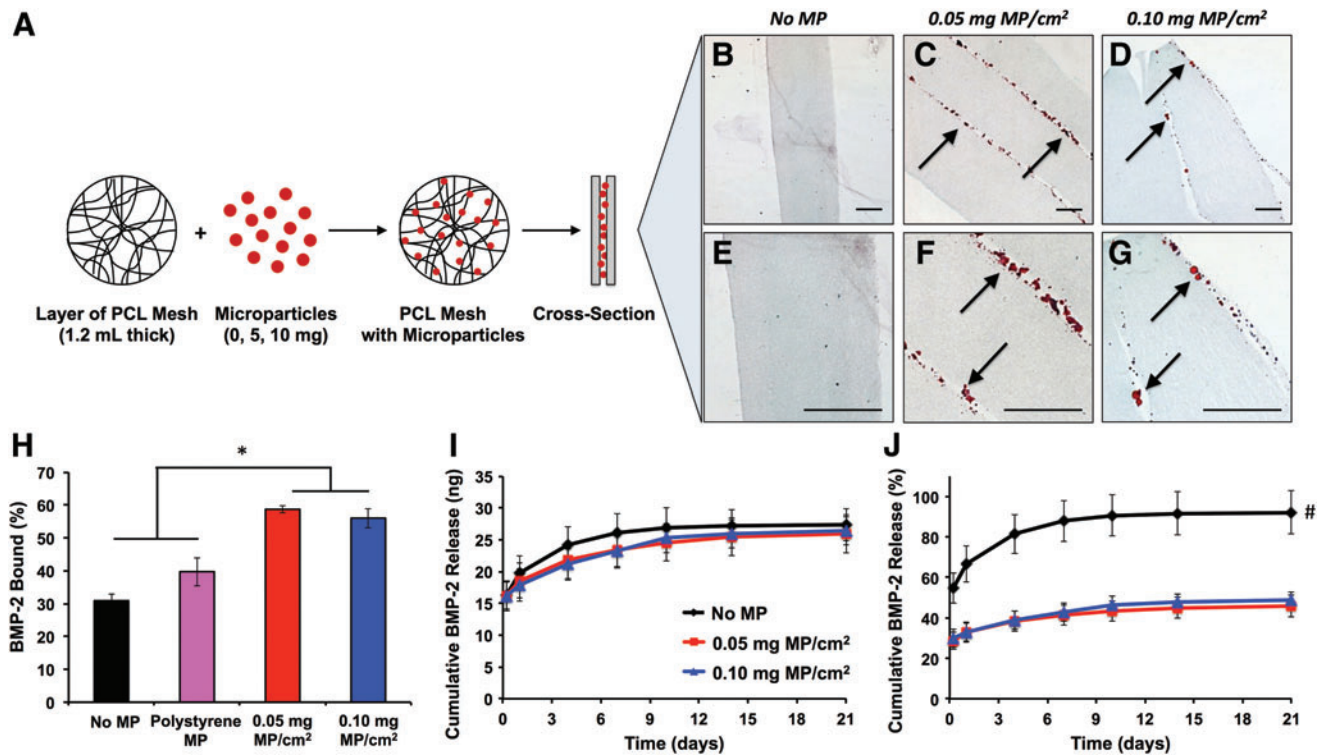
FIG. 1. Fabrication and characterization of heparin microparticle-containing polycaprolactone nanofiber meshes. **(A)** Schematic of microparticle-containing mesh fabrication. **(B–D)** Low-magnification images of mesh cross-sections stained with Safranin O and Fast Green demonstrated microparticles distributed throughout two layers in microparticle-containing meshes. **(E–G)** High-magnification images of mesh cross-sections stained with Safranin O and Fast Green. All scale bars = 100 μm. **(H)** Six-millimeter-diameter mesh pieces loaded with 100 ng of BMP-2 over 16 h at 4°C demonstrated higher BMP-2 binding in the presence of heparin microparticles compared with no microparticles and polystyrene microparticles. (*$p < 0.05$ as indicated.) **(I)** Cumulative mass of BMP-2 release over 21 days was similar between meshes without microparticles and meshes with heparin microparticles. **(J)** Cumulative BMP-2 release as a percentage of initial loading was higher for meshes without microparticles compared with meshes containing microparticles (#$p < 0.05$ compared with 0.05 and 0.10 mg MP/cm^2 meshes at each time point.). BMP-2, bone morphogenetic protein-2; MP, microparticles. Color images available online at www.liebertpub.com/tea

(8 mm). Mesh tubes underwent 100% ethanol evaporation overnight, followed by disinfection in 70% ethanol for 4 h, and finally immersion in sterile PBS until surgery.

Microparticle-containing PCL mesh characterization

Six-millimeter-diameter disks from representative meshes were embedded in cryomedium, and 5 μm cross-sections were taken along the disk diameter for histological analysis. Sections were stained with Safranin O and Fast Green to visualize heparin microparticle distribution within each mesh. Images of meshes were taken on a Zeiss Axio Observer Z.1 inverted microscope with Zeiss AxioVision software (Zeiss, Oberkochen, Germany).

In vitro *BMP-2 binding and release from meshes*

To evaluate *in vitro* BMP-2 binding and release, 6-mm-diameter disks from each mesh were incubated in a solution of 100 ng of BMP-2 (Pfizer, New York, NY) in 1 mL of 0.1% (w/v) bovine serum albumin (BSA; Sigma-Aldrich) in PBS with gentle mixing (Tube Revolver/Rotator; Thermo Fisher Scientific) for 16 h at 4°C. Meshes were then removed, and the remaining solution was evaluated for BMP-2 content by using an enzyme-linked immunosorbent assay

(ELISA; R&D Systems, Minneapolis, MN). The mass of BMP-2 bound to meshes was determined by normalizing unbound BMP-2 to a solution of 100 ng of BMP-2 incubated for 16 h at 4°C without microparticles. BMP-2-loaded meshes were then placed in 1 mL of fresh solution and incubated at 37°C for a period of 21 days to measure passive BMP-2 release from the meshes. After 0.25, 1, 4, 7, 10, 14, and 21 days, the entire solution was removed and replaced with 1 mL of fresh 0.1% BSA in PBS. Samples were evaluated for BMP-2 content via ELISA. In all binding and release assays, BSA addition and low-binding tubes (Axygen Maxymum Recovery; Corning Mediatech) were used to minimize nonspecific BMP-2 binding to surfaces.

Rat femoral segmental defect procedure

Surgeries were performed on 13-week-old female SASCO Sprague–Dawley rats (∼250 g) as previously described,[38] using procedures approved by the Georgia Institute of Technology Institutional Animal Care and Use Committee. A custom radiolucent fixation plate (polysulfone) with two stainless steel risers at the ends was attached directly onto the femur for stabilization. An oscillating saw was used to create an 8-mm-long, critically sized, full-thickness mid-diaphyseal defect. Each defect was treated with a bovine collagen sponge

(L = 10 mm, D = 5 mm; Kensey Nash, Exton, PA) that was soaked with 30 μg of BMP-2 in 150 μL of 0.1% (w/v) rat serum albumin (RSA) in 4 mM hydrochloric acid, inserted into a PCL nanofiber mesh tube (L = 12 mm, D = 5 mm), and fit into the defect. Images of a model segmental defect treated with a collagen sponge and PCL mesh tube can be found in Supplementary Figure S1 (Supplementary Data are available online at www.liebertpub.com/tea). The following PCL mesh formulations were tested *in vivo*: (1) no heparin microparticles, (2) meshes with 0.05 mg MP/cm^2 (0.11 mg heparin microparticles total), (3) meshes with 0.10 mg MP/cm^2 (0.23 mg microparticles total), (4) meshes with 0.9 mm perforations without heparin microparticles, and (5) meshes with 0.9 mm perforations and 0.10 mg MP/cm^2 (0.23 mg heparin microparticles total, before perforation).

In vivo *radiography and micro-computed tomography*

Longitudinal *in vivo* radiographs were obtained at 2, 4, 8, and 12 weeks postsurgery (Faxitron MX-20; Faxitron Bioptics, LLC, Tucson, AZ) at a voltage of 23 kV and an exposure time of 15 s. *In vivo* micro-computed tomography (μCT) was conducted at 4, 8, and 12 weeks postsurgery (Viva CT; Scanco, Brüttisellen, Switzerland) to quantify bone volume and mineral density. Animals were scanned at a voxel size of 38.5 μm, voltage of 55 kVp, current of 109 μA, and medium resolution. Mineral was quantified within the central ~6 mm (160 scan slices) of each 8 mm defect, and three different volumes of interest were identified: (1) total mineral volume of the thigh within the region of interest, (2) mineral volume within the defect space, as defined by 5 mm-diameter circular contours corresponding to the diameter of the nanofiber mesh, and (3) heterotopic mineral volume, which fell outside of the 5 mm diameter circular contours. A global threshold for newly regenerated bone was set at 50% of the mineral density of native cortical bone, and a Gaussian filter (sigma = 1.2, support = 1) was applied to suppress noise.

Biomechanical testing

Femora for mechanical testing were harvested from animals at 12 weeks and stored at −20°C. Immediately before testing, samples were thawed to room temperature, and soft tissue and polysulfone fixation plates were removed, leaving the metal risers attached to the bone. The bone ends (including part of the metal risers) were potted in molten Wood's metal (Alfa Aesar, Haverhill, MA) in custom metal holders, allowed to solidify, and mounted in the test clamps. Torsion was applied at a rate of 3° per second until failure on a torsion testing system (Bose EnduraTEC ELF200; Bose Electroforce Systems Group, Eden Prairie, MN), allowing for the determination of maximum torque and calculation of torsional stiffness, using the slope of the linear segment of the torque-rotation curve. Seven to eight samples from each treatment group and five contralateral intact femora were tested.

Histological analysis of bone regeneration

One representative femur from each treatment group was isolated for histology at 12 weeks postsurgery. After harvesting, the femora were fixed in 10% neutral buffered formalin at 4°C for 24 h, followed by decalcification (Cal Ex-II; Fisher Scientific, Pittsburgh, PA) with gentle agitation for 14 days. Samples were dehydrated through submersion in a series of alcohol and xylene solutions and vacuum-embedded in paraffin wax at 60°C; 5–7 μm midsagittal sections of the defects were stained with Safranin O and Fast Green, to identify heparin microparticles within the mesh. Images of sections were taken on a Zeiss Axio Observer Z.1 inverted microscope with Zeiss AxioVision software.

In vitro *BMP-2 binding and release from heparin microparticles*

Contact time required for BMP-2 binding to heparin microparticles. *In vitro* evaluation of BMP-2 binding and release from heparin microparticles was performed as previously described.[35] 0.1 mg of microparticles was incubated with 100 ng of BMP-2 in 1 mL of 0.1% BSA in PBS at 4°C for a maximum of 16 h, to investigate the minimum time required for BMP-2 binding to microparticles.

Competitive binding of serum components to heparin microparticles. To determine whether serum borne biomolecules interfered with BMP-2 binding to microparticles, microparticles (10 μg) were incubated with a range of BMP-2 concentrations (3–3000 ng/mL) in 1 mL of fetal bovine serum (FBS; Hyclone–GE Healthcare Life Sciences, Logan, UT) or 0.1% BSA in PBS for 16 h at 37°C. BMP-2 content of microparticle-containing samples was normalized to samples containing BMP-2 alone in 0.1% BSA in PBS or FBS and incubated for 16 h at 37°C. BMP-2 release (100 ng) from heparin microparticles (0.1 mg) was evaluated in both 0.1% BSA/PBS and FBS at 37°C over 21 days. At each time point, the entire solution was removed and replaced with 1 mL of fresh solution. All samples were evaluated for BMP-2 content via ELISA.

Polyacrylamide gel electrophoresis analysis

Protein binding to heparin microparticles was confirmed by sodium dodecyl sulfate polyacrylamide gel electrophoresis (SDS-PAGE) followed by silver staining for all protein bands. Next, 0.1 mg of microparticles was incubated in PBS, 30 ng of BMP-2 in 0.1% BSA in PBS, FBS, or 30 ng of BMP-2 in FBS at 4°C for 16 h. Microparticles were then centrifuged, washed once with PBS, and resuspended in SDS-PAGE loading buffer. Thirty nanograms of soluble BMP-2 in 0.1% BSA in PBS and diluted FBS (1:25, 1:50) were also resuspended in loading buffer as additional controls. All solutions were heated to 95°C for 10 min before loading onto a 12% Mini-PROTEAN TGX gel (Bio-Rad Laboratories, Hercules, CA). Gel electrophoresis was performed in SDS-PAGE running buffer by using a Mini-PROTEAN Tetra Cell system (Bio-Rad Laboratories) set at a constant voltage (200 V) for 40 min. A 10–250 kDa protein ladder (Precision Plus Kaleidoscope; Bio-Rad Laboratories) was used as a molecular weight reference. Silver staining of SDS-PAGE gels was performed by using the Silver Staining Plus Kit (Bio-Rad Laboratories) as per the manufacturer's instructions.

Mass spectrometry of heparin microparticle samples

To identify serum proteins bound to microparticles, mass spectrometry analysis was performed on microparticles (1 mg) that were loaded with 5 mL of FBS or 5 mL of FBS and 8 µg BMP-2 together by using aforementioned techniques. The microparticles were centrifuged, washed once with PBS, and proteins bound to microparticles were digested with 2 units of glutamyl endopeptidase (Glu-C; EMD Millipore, Darmstadt, Germany) for 16 h and 10 units of lysyl endopeptidase (Lys-C; Wako Chemicals USA, Richmond, VA) for 3.5 h in 50 mM HEPES (pH = 7.9). Eluted peptides were purified, dried, and resuspended in a 5% acetonitrile and 4% formic acid solution for liquid chromatography-tandem mass spectrometry (LC-MS/MS) analysis. Detailed mass spectrometry methods can be found in the Supplementary Data.

Statistical analysis

All data are reported as mean ± standard error of the mean. *In vitro* experiments were run with a minimum of three replicates for each experimental group and repeated at least three times. For BMP-2 binding and release from nanofiber meshes, 3–10 meshes were analyzed from each group with three replicates. For *in vivo* bone defect experiments, longitudinal µCT was conducted on eight to nine femora per group, and endpoint biomechanical testing was conducted on seven to eight femora per group. Statistical significance was determined by using one-way or two-way analysis of variance (ANOVA), as appropriate, followed by Bonferroni's *post hoc* analysis (Graphpad Prism, Version 5.0, La Jolla, CA). For data that did not satisfy the assumptions of equal variances and Gaussian distributions, the Kruskal–Wallis test was used. $p < 0.05$ was considered statistically significant.

Results

Microparticle-containing PCL mesh characterization

Cross-sections of PCL nanofiber meshes stained with Safranin O and Fast Green revealed two layers of heparin microparticles (red) between PCL layers (gray) in both 0.05 mg MP/cm^2 meshes (Fig. 1C, F) and 0.10 mg MP/cm^2 meshes (Fig. 1D, G). Meshes without microparticles consisted of a single continuous PCL layer (Fig. 1B, E). Some mesh delamination and microparticle loss was observed in the 0.10 mg MP/cm^2 meshes, demonstrated by separation of the mesh layers and presence of microparticles at the mesh surface (Fig. 1D, G); this may have been caused by the ethanol spray step in the fabrication technique or histology processing. Meshes that exhibited delamination during manipulation before *in vivo* implantation were excluded from the study.
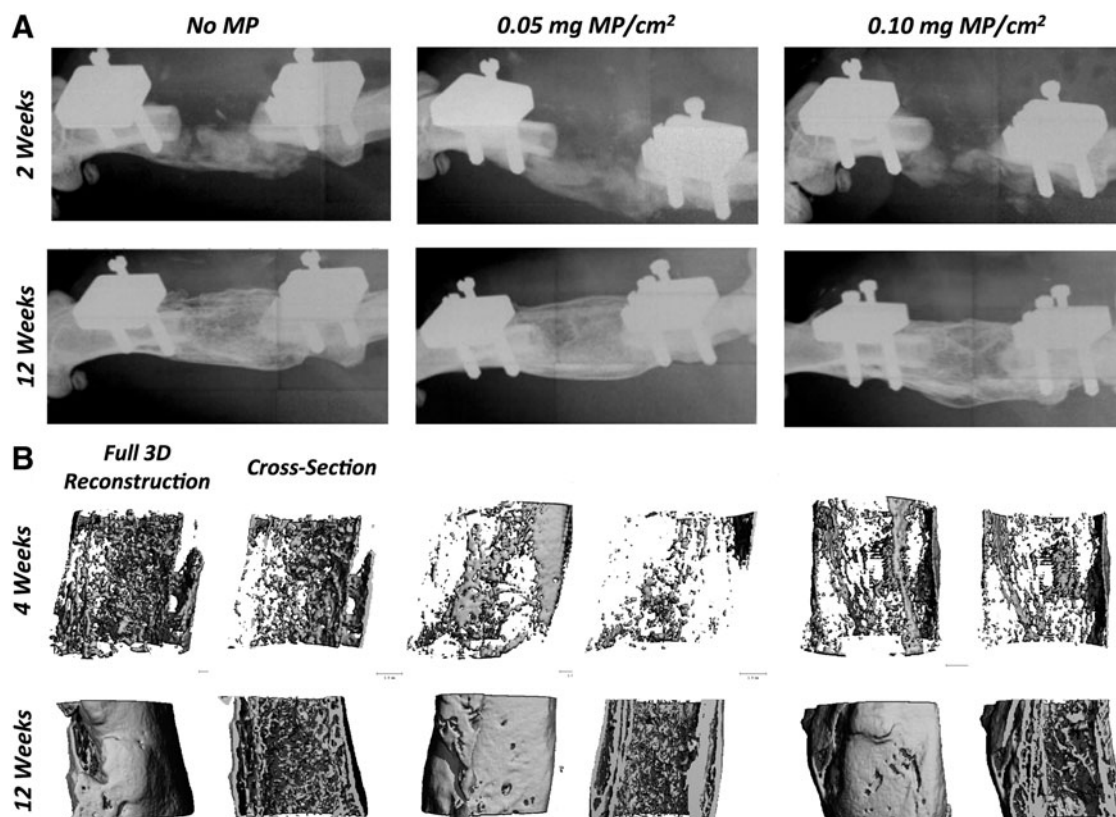

FIG. 2. Representative radiographs and three-dimensional µCT reconstructions of bone defects at 2, 4, and 12 weeks postsurgery. **(A)** Radiographs and **(B)** µCT reconstructions (full reconstructions and cross-sections) of defects treated with No MP, 0.05, and 0.10 mg MP/cm^2 meshes depicted heterotopic ossification as early as 2 weeks postsurgery that persisted until 12 weeks. Complete bridging was achieved in 9/9 of No MP mesh, 8/9 of 0.05 mg MP/cm^2 mesh, and 8/8 of 0.10 mg MP/cm^2 mesh treated defects. µCT, micro-computed tomography.

BMP-2 binding and release from meshes

PCL nanofiber meshes containing 0.05 and 0.10 mg/cm^2 of heparin microparticles depleted more BMP-2 from solution ($58.7\% \pm 1.1\%$, $56.0\% \pm 3.0\%$, respectively) than meshes without heparin microparticles or with 0.05 mg/cm^2 of uncharged 4 μm polystyrene microparticles without electrostatic affinity for BMP-2 ($30.9\% \pm 2.0\%$, $39.7\% \pm 4.3\%$, respectively; $n = 4–10$, $p < 0.05$) when loaded with 100 ng of BMP-2 in 0.1% BSA in PBS (Fig. 1H). Meshes with and without microparticles exhibited similar BMP-2 release profiles, releasing 25–27 ng of BMP-2 after 21 days *in vitro*

(Fig. 1I). However, when BMP-2 release was evaluated as a percentage of initial BMP-2 loading, meshes without microparticles released almost all of the bound BMP-2 ($88.6\% \pm 10.3\%$), compared with meshes with 0.05 and 0.10 mg/cm^2 of heparin microparticles, which released less than half of the bound BMP-2 over 21 days ($44.1\% \pm 5.1\%$ and $47.2\% \pm 4.0\%$, respectively; $p < 0.001$) (Fig. 1J). Since the majority of the loaded BMP-2 was retrieved from meshes without microparticles, the incomplete release of BMP-2 from microparticle-containing meshes was likely due to BMP-2 remaining within the meshes and not due to protein degradation.
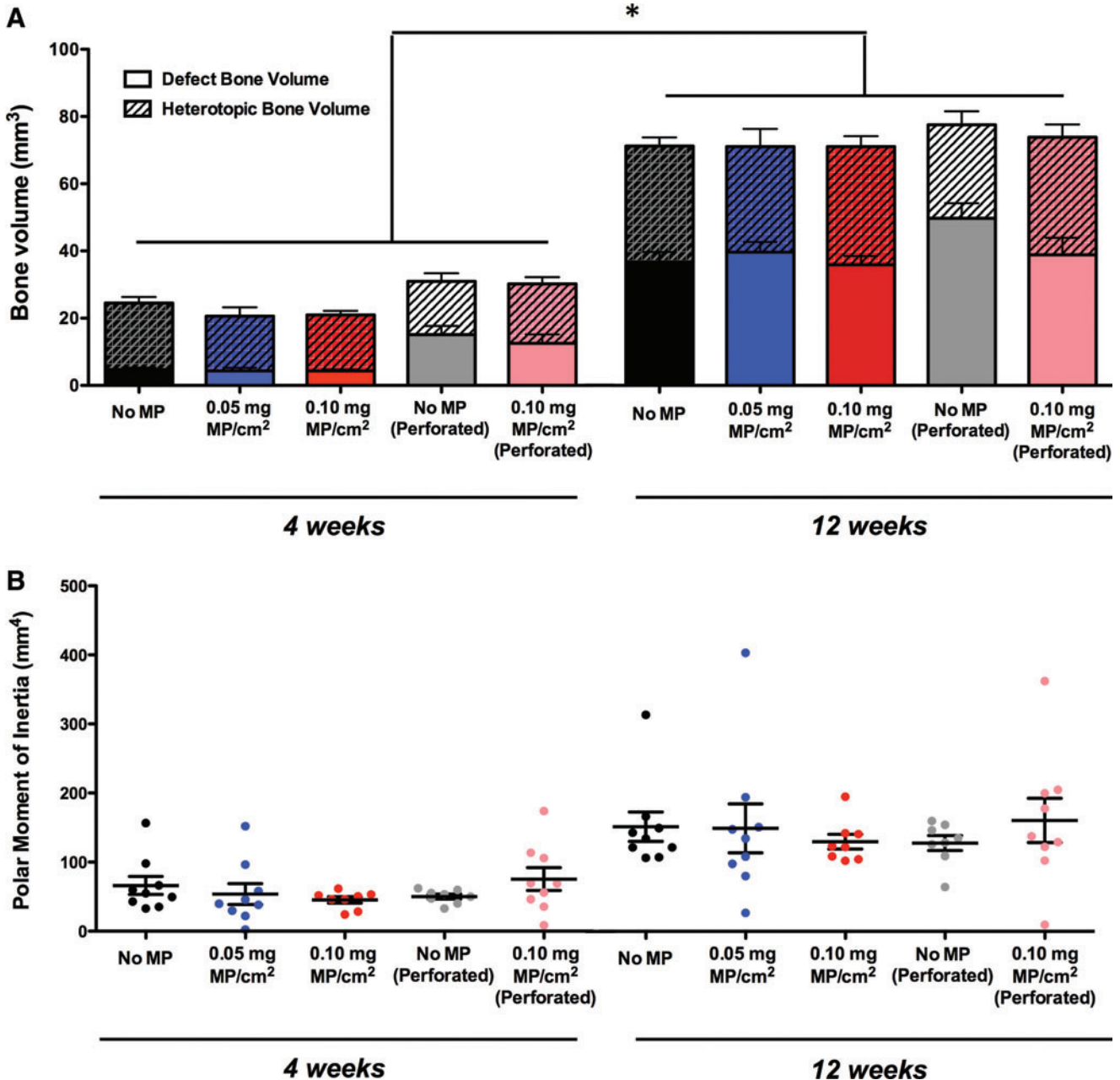

FIG. 3. Quantitative μCT analysis of bone defects after 4 and 12 weeks. **(A)** Defect bone volume (*solid bars*), heterotopic bone volume (*diagonal line bars*), and total bone volume (*combined bars*) were not different between treatment groups. Bone volume in each group increased over time ($p < 0.05$ as indicated). **(B)** Polar moment of inertia was calculated to determine the distribution of newly formed bone from the central axis of the femur and was also not different between groups. Color images available online at www.liebertpub.com/tea
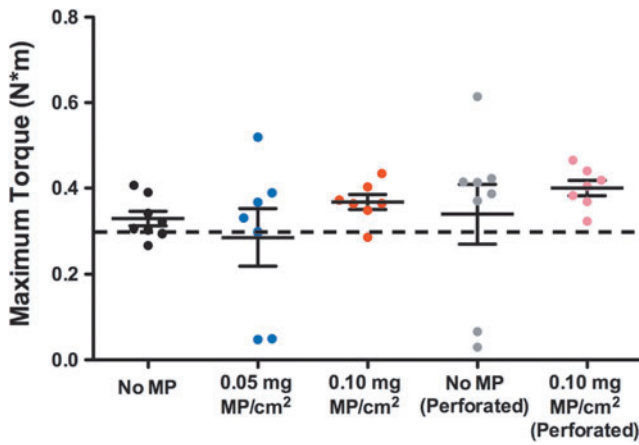
FIG. 4. Biomechanical properties of regenerated bone at 12 weeks. Regenerated femora underwent torsion testing to failure after 12 weeks postsurgery. Maximum torque was not different between groups or compared with that of intact femora (*dashed line*). Color images available online at www.liebertpub.com/tea

Bone regeneration and biomechanical properties

Progressive mineralization in and around the bone defect area occurred in all groups over time (Fig. 2A and Supplementary Fig. S2A), resulting in robust bony bridging in nearly all samples after 12 weeks (9/9 of No MP, 8/9 of 0.05 mg MP/cm^2, 8/8 of 0.10 mg MP/cm^2, 8/8 of Perforated No MP, and 8/9 of Perforated 0.10 mg MP/cm^2). Heterotopic ossification outside of the defect area was observed in all groups as early as 2 weeks postsurgery and persisted through 12 weeks. Overall, no qualitative reduction in heterotopic ossification was observed with the inclusion of heparin microparticles in PCL meshes (Fig. 2). In addition, no abnormal bleeding was observed in any animals during

and after the surgical procedure, regardless of the presence of heparin microparticles.

Heterotopic ossification was observed in all treatment groups regardless of mesh type (Fig. 2B and Supplementary Fig. S2B). Mineralization within the defect site increased in all groups over time, with no differences in total bone volume, defect bone volume, or heterotopic bone volume between groups at each time point (Fig. 3A). The polar moment of inertia was calculated to evaluate the spatial distribution of bone from the central axis of the femur and was not found to be different between groups (Fig. 3B). Similarly, no notable morphological differences in the regenerated bone were observed (Supplementary Fig. S3). Finally, biomechanical properties (maximum torque [Fig. 4] and torsional stiffness [Supplementary Fig. S4]) were comparable between all groups and did not differ from the properties of age-matched intact femora.

Histological analysis of femora

Heparin microparticles remained entrapped within the mesh after 12 weeks *in vivo* (Fig. 5; indicated by red arrows); microparticles were readily distinguishable from endogenous GAGs due to their punctate, circular appearance and dark red staining. Mesh integrity was better maintained in the 0.05 mg MP/cm^2 meshes, which exhibited two distinct layers of microparticles and were comparable in appearance to intact meshes before implantation, suggesting long-term maintenance of microparticles *in vivo* (Fig. 5B, E). However, some areas of mesh disintegration were observed. The 0.10 mg MP/cm^2 meshes displayed greater mesh delamination, as illustrated by large gaps within the meshes and an overall expansion of mesh area. Some microparticles were located in close proximity to the 0.10 mg MP/cm^2 meshes (indicated by red arrow, Fig. 5C) or entrapped within it (Fig. 5F), but microparticle retention was not observed to
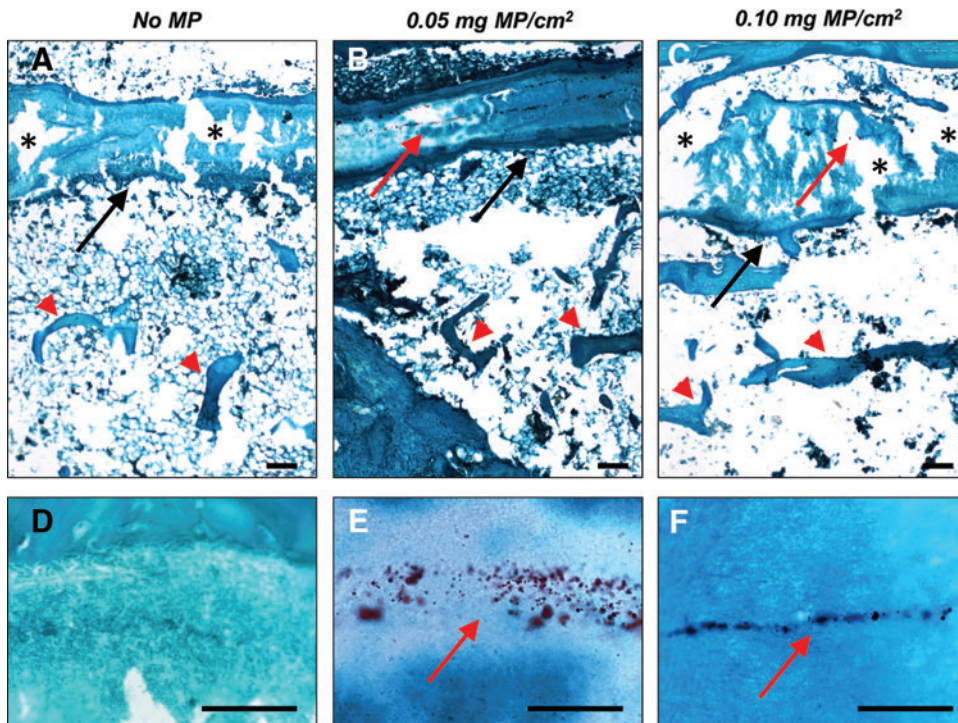

FIG. 5. Safranin O and Fast Green staining of bone defects at 12 weeks. Safranin O and Fast Green staining was performed on defects treated with **(A, D)** No MP meshes, **(B, E)** 0.05 mg MP/cm^2 meshes, and **(C, F)** 0.10 mg MP/cm^2 meshes. *Black arrows* denote the mesh boundary, and *red arrowheads* denote areas of the new bone. Heparin microparticles, which are denoted by *red arrows*, were found entrapped within 0.05 and 0.10 mg MP/cm^2 meshes. Areas of mesh delamination are indicated by *asterisks*; 0.10 mg MP/cm^2 meshes demonstrated more delamination than other meshes. All scale bars = 100 μm. Color images available online at www.liebertpub.com/tea

the same extent as with the 0.05 mg MP/cm² meshes. Notably, heparin microparticles were not observed outside of the nanofiber mesh boundary (indicated by black arrows), in the defect region, or in surrounding muscle. Overall, the regenerated bone demonstrated a trabecular structure (indicated by red arrowheads) interspersed with areas of loose fibrous tissue, as has been previously observed with collagen sponge delivery of BMP-2 in this model.[39]

Effect of incubation time on BMP-2 binding to heparin microparticles

Since the presence of heparin microparticles in the PCL meshes did not have an impact on bone regeneration *in vivo*, the minimal time required for BMP-2 binding to microparticles was evaluated *in vitro* over 16 h. It was observed that $64.1\% \pm 6.5\%$ of the BMP-2 incubated with microparticles bound to the microparticles immediately after contact and increased to $83.3\% \pm 4.3\%$ within the first hour (Fig. 6A).

BMP-2 binding continued to increase over the next 4 h before reaching a plateau of $\sim 90\%$ BMP-2 binding, after which additional incubation time did not increase BMP-2 binding to microparticles.

Competitive binding of serum components and BMP-2 to heparin microparticles

Because contact between BMP-2 and microparticle-containing meshes *in vivo* occurred in the presence of numerous blood borne factors, which could interfere with BMP-2-heparin interactions, *in vitro* BMP-2 binding and release experiments were performed in the presence of serum and compared with results obtained in 0.1% (w/v) BSA in PBS. Overall, heparin microparticles bound less BMP-2 in the presence of FBS when loaded at BMP-2 concentrations between 3 and 3000 ng/mL (corresponding to 0.3–300 µg of BMP-2 per mg of microparticles) (Fig. 6B). Microparticles loaded with BMP-2 in 0.1% BSA in PBS
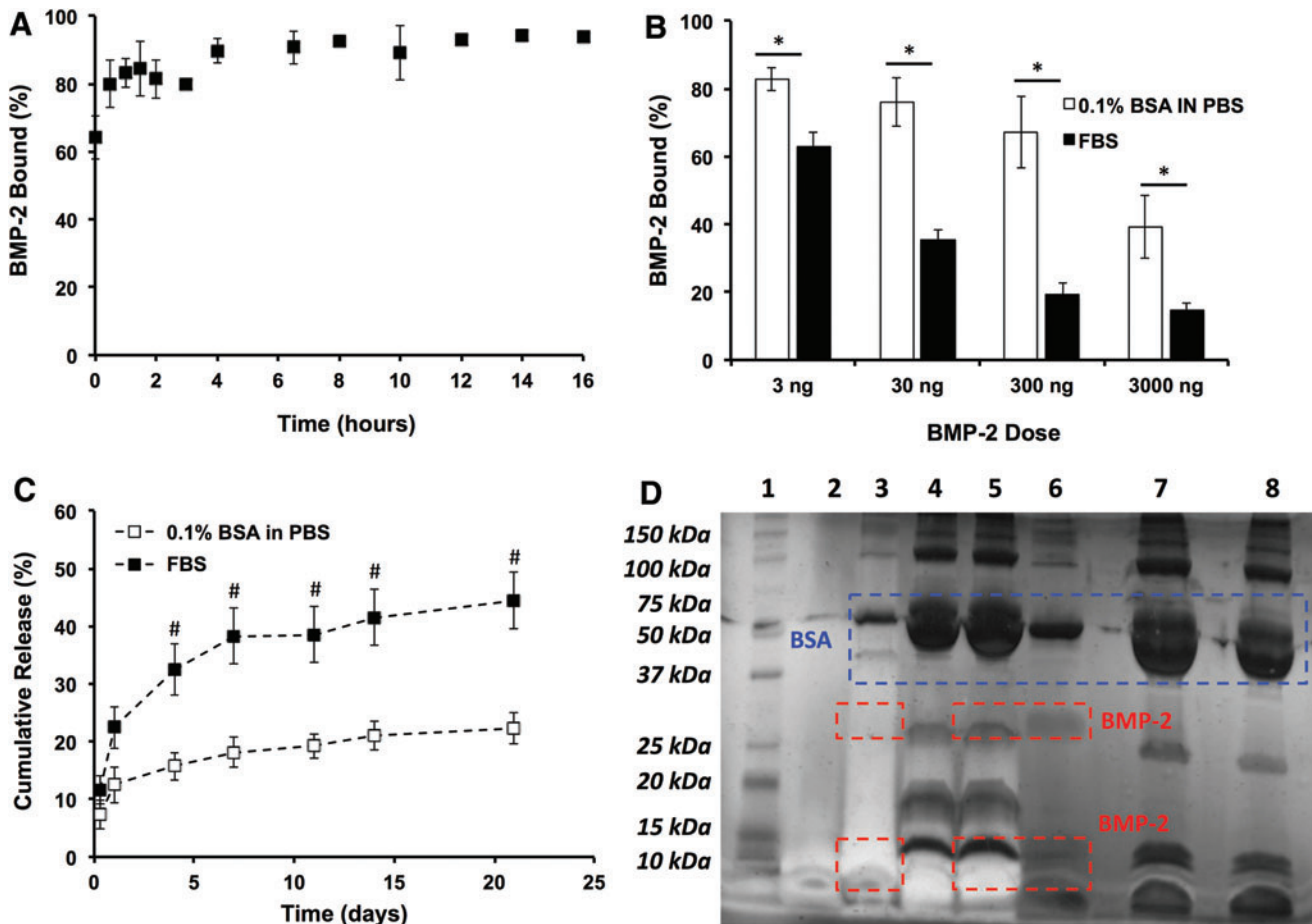

FIG. 6. Effect of contact time and presence of serum on BMP-2 binding and release from heparin microparticles. **(A)** 0.1 mg of heparin microparticles loaded with BMP-2 over different periods of time exhibited >60% BMP-2 binding immediately on contact and a maximum binding of $\sim 90\%$ after 4 h. **(B)** Ten micrograms of heparin microparticles loaded with 3–3000 ng of BMP-2 over 16 h at 37°C demonstrated reduced binding in the presence of FBS compared with 0.1% BSA in PBS (*$p < 0.01$ as indicated). **(C)** When 0.1 mg of heparin microparticles was loaded with 100 ng of BMP-2 and allowed to release BMP-2 into 0.1% BSA in PBS or FBS, cumulative release of BMP-2 was higher in FBS after 4 days (#$p < 0.05$ between 0.1% BSA in PBS and FBS at indicated time points). **(D)** Gel electrophoresis followed by silver staining was completed in the following samples: (1) ladder, (2) unloaded MPs, (3) MPs loaded with 30 ng of BMP-2, (4) MPs loaded with FBS, (5) MPs loaded with FBS +30 ng of BMP-2, (6) 30 ng of soluble BMP-2, (7) FBS diluted 1:25, and (8) FBS diluted 1:50. *Blue dashed box* indicates BSA bands, and *red dashed boxes* indicate BMP-2 monomer and dimer bands. BSA, bovine serum albumin; FBS, fetal bovine serum; PBS, phosphate-buffered saline. Color images available online at www.liebertpub.com/tea

TABLE 1. SELECTED PEPTIDES FROM KNOWN HEPARIN BINDING PROTEINS IDENTIFIED
ON FETAL BOVINE SERUM-LOADED HEPARIN MICROPARTICLES

Protein	Peptide	ppm	XCorr
Apolipoprotein-A1	D.NWDTLASTLSK.V	1.03	3.3
	E.TLRQQLAPYSDD.L	0.63	2.9
	E.QLGPVTQE.F	0.27	2.6
Apolipoprotein-B	E.TSRSLPYAQNIQDQLSGLQE.L	1.30	5.9
	K.VSDSLIGVTQGYSVTVK.H	−0.28	4.5
	E.ITVPASQLTVSQFTLPK.S	0.77	4.1
Apolipoprotein-C2	K.TYLPAVDEK.I	0.55	2.4
	D.QVFSVLSGKD.-	0.71	2.0
	E.SLLGYWDTAK.A	0.83	2.9
Apolipoprotein-E	E.LQAAQARLGSDME.D	0.64	4.6
	D.YLRWVQTLSDQVQE.E	−0.06	4.3
	E.QGQSRAATLSTLAGQPLLE.R	0.73	3.8
Thrombospondin-1	K.DHSGQVFSVISNGK.A	−0.37	4.8
	K.FQDLVDAVRAE.K	0.45	3.6
	K.GPDPSSPAFRIE.D	0.83	3.1
Thrombospondin-4	E.FQTQNFDRLD.K	−0.13	2.4
	K.SSATIFGLYSSADHSK.Y	0.70	2.3
	K.SSATIFGLYSSADHSK.Y	0.04	3.8
Fibronectin-1	K.LGVRPSQGGEAPRE.V	0.62	4.4
	E.SLPLVGQQSTVSDVPRDLE.V	0.04	4.2
	E.YVYTISVLRDGQE.R	−0.21	4.2

Ppm indicates mass accuracy, and XCorr indicates correlation between experimental and theoretical mass spectra for each peptide.

bound ~75% of the BMP-2 at lower doses, whereas binding was reduced to $39.3\% \pm 9.3\%$ at the highest dose ($300 \mu g$ BMP-2/mg MPs); the BMP-2 binding efficiencies obtained in 0.1% BSA in PBS at higher growth factor concentrations were similar to results documented in our previous publication.[35] In contrast, microparticles loaded with BMP-2 in the presence of FBS bound significantly less BMP-2 at each dose, with the highest loading percentage at the lowest dose ($63.0\% \pm 3.9\%$ compared with $82.8\% \pm 3.3\%$ in BSA/PBS; $p < 0.01$) and the lowest loading percentage at the highest dose ($14.7\% \pm 2.2\%$ compared with $39.3\% \pm 9.3\%$ in BSA in PBS, $p < 0.01$). Similarly, the presence of FBS during BMP-2 release from microparticles doubled the amount of BMP-2 released after 21 days ($44.4\% \pm 8.4\%$ compared with $22.3\% \pm 4.6\%$; $p < 0.05$) (Fig. 6C).

Gel electrophoresis and mass spectrometry were performed to identify the serum proteins interfering with BMP-2-heparin interactions. Silver staining of SDS-PAGE gels revealed BMP-2 monomer and dimer bands (red boxes) in the soluble BMP-2 lane (No. 6) at ~13 and ~26 kDa, respectively, as well as a BSA band (blue box) at ~63 kDa (Fig. 6D). The BMP-2 monomer (red box) and BSA (blue box) bands were also visible in the BMP-2-loaded microparticle lane (No. 3), although no BMP-2 dimer band was observed and the bands were considerably less intense, indicating, as expected, incomplete binding of BMP-2 to the microparticles. The BSA bands in the FBS-loaded microparticle lanes (No. 4, No. 5) were found to be similar in size to those of the 1:50 diluted FBS lane (No. 8), demonstrating that only a fraction of the BSA in FBS bound to heparin microparticles. Interestingly, several distinct bands emerged in the FBS-loaded microparticle lanes between 15 and 37 kDa, which were not present in the diluted FBS lanes, suggesting the concentration of multiple proteins within this molecular weight range. When microparticles were loaded with BMP-2

in the presence of FBS (No. 5), similar protein bands were observed compared with FBS loading alone; however, the BMP-2 monomer band was faint in comparison, suggesting that serum proteins were preferentially binding to the microparticles in a much higher abundance than BMP-2.

Mass spectrometry was used to identify proteins on FBS-loaded heparin microparticles. All proteins detected on FBS-loaded microparticles are listed in Supplementary Table S1. Proteins identified based on only two or fewer unique peptides were excluded from the analysis. Out of the 33 total proteins identified, 20 were known heparin-binding proteins, including several apolipoproteins and thrombospondins. Selected peptides identified from these heparin-binding proteins are highlighted in Table 1. XCorr signifies the correlation between the experimental mass spectra and theoretical mass spectra of the peptide, whereas the mass accuracy of each peptide demonstrates how closely the theoretical mass of the peptide matches the experimentally measured mass. The extracellular matrix protein fibronectin, which has a known heparin binding site and a specific affinity for heparin,[40] was confidently identified based on 26 unique peptides. On microparticles loaded with both FBS and BMP-2, BMP-2 was only identified based on one unique peptide and, thus, was not included in the list of detected proteins. This further suggests that FBS-borne proteins bound to the microparticles in larger quantities than BMP-2, and this corroborates the results obtained from SDS-PAGE analysis.

Discussion

Poor BMP-2 localization after delivery is a limiting factor in the widespread use of BMP-2 therapy for bone-healing applications. Most delivery approaches have focused on the controlled release of growth factors from scaffolds through either nonspecific electrostatic binding, which may result in

rapid growth factor dissociation, or covalent localization, which may reduce growth factor bioactivity.[5,41] In this study, we designed a hybrid nanofiber mesh barrier containing entrapped heparin microparticles with the goal of creating a growth factor sink to impede BMP-2 diffusion outside of the site of interest and to reduce the incidence of heterotopic ossification *in vivo*. The addition of microparticles into the nanofiber meshes resulted in increases in BMP-2 binding capacity and decreases in BMP-2 release from the meshes. Despite promising results achieved *in vitro*, the microparticle-containing meshes did not perform as hypothesized *in vivo*, since no significant impact was observed on heterotopic ossification, regenerated bone volume, or mechanical properties.

With its high affinity for BMPs, heparin was previously incorporated into a number of biomaterial scaffolds to provide BMP-2 sustained delivery *in vivo*.[28–34] Unlike most heparin-containing biomaterials, which are typically used to deliver BMP-2 to bone defects, we employed heparin microparticles entrapped within PCL nanofiber meshes as a strategy to localize BMP-2 release from the clinical collagen sponge. This biomimetic concept of using heparin as a growth factor sink resembles the natural role played by other GAGs (heparan sulfate and chondroitin sulfate) during development, in which areas of high GAG content sequester cell-secreted growth factors, such as fibroblast growth factors (FGFs) and BMPs, to localize mitogenic and morphogenic cues.[42] Although a few other studies have used empty heparin materials to sequester cell-secreted growth factors,[43,44] to our knowledge, this is the first study that demonstrates the use of an empty heparin biomaterial to locally sequester co-delivered BMP-2 *in vivo*.

The fact that the hybrid mesh exhibited favorable BMP-2 binding and release kinetics *in vitro*, but could not spatially control bone distribution *in vivo*, could be due to a number of reasons. Inadequacies in the physical mesh barrier itself (irrespective of the presence of microparticles) may have contributed to the patterns of bone formation observed. First, the mesh tubes did not fit tightly around the bone ends, as shown in Supplementary Figure S1, potentially allowing BMP-2 to exit the collagen sponge without contacting the embedded microparticles; second, the possible delamination of these meshes *in vivo* may have further disrupted the intended barrier. Despite these scaffold limitations, heterotopic ossification was not limited to the bone ends alone (Fig. 2 and Supplementary Fig. S2), and was also evident in femora treated with $0.05 \, mg \, MP/cm^2$ meshes, which remained intact with localized microparticles throughout the 12-week study (Fig. 5). Furthermore, even with the loss of mesh integrity observed in the $0.10 \, mg \, MP/cm^2$ meshes, microparticles were observed within the mesh region, accessible to diffusing BMP-2. Mesh perforations, which accelerated early mineralization at a lower BMP-2 dose ($5 \, \mu g$) in alginate by facilitating vascular ingrowth and cell infiltration,[37] did not impact early bone formation in this study, potentially due to the increased BMP-2 dose and use of a collagen sponge with low BMP-2 affinity. No abnormal bleeding was observed in response to the use of heparin microparticles, both during the surgical procedure and in the weeks after treatment. This suggested that cross-linked heparin microparticles embedded within the nanofiber meshes did not possess the anticoagulant abilities of linear, soluble heparin.

We also sought to investigate the conditions under which the microparticles entrapped within the mesh tubes would contact and bind BMP-2 *in vivo* and how this differed from our initial *in vitro* investigation. Contact time between microparticles and BMP-2 did not appear to play an important role *in vitro*, as >60% of the BMP-2 in solution bound to the microparticles immediately on contact and only 4 h of incubation were required for >90% binding. This suggested that BMP-2 released from the collagen sponge could readily bind to the hybrid mesh. On the other hand, the presence of bovine serum decreased the BMP-2 binding capacity of the microparticles and promoted BMP-2 release.

In our previous publication, heparin microparticles displayed a maximum binding capacity of $\sim 300 \, \mu g$ BMP-2 per mg of microparticles in 0.1% BSA in PBS.[35] Based on this binding capacity, the density of microparticles embedded in the meshes (0.11–0.23 mg MPs/mesh) should have been sufficient to capture the entire mass of BMP-2 delivered ($30 \, \mu g$). However, given the reduced BMP-2 binding capacity of heparin microparticles in the presence of FBS *in vitro*, the binding capacity of the microparticles *in vivo* may have also been reduced in the presence of blood-borne soluble factors in the bone defect environment. At the highest BMP-2 dose evaluated *in vitro* ($300 \, \mu g$ BMP-2/mg MPs), the BMP-2 binding capacity of the microparticles was reduced by >60% in the presence of FBS. Moreover, BMP-2 release from the microparticles in the presence of serum was double that of BMP-2 release in 0.1% BSA in PBS over 21 days.

Rapid adsorption of blood-borne proteins to biomaterial surfaces on implantation is a well-documented phenomenon that has been observed with many different materials, including metals, glass, and polymers.[45,46] The kinetics of protein binding from blood have been described by the Vroman Effect, in which proteins that are more mobile and abundant, such as albumin, immunoglobins, globulins, fibrinogen, and fibronectin, adsorb to the material immediately, followed by slower replacement with larger proteins that have a higher affinity for the material.[45,47] Our *in vitro* experiments involving incubation of heparin microparticles in FBS were conducted over several hours or days, allowing ample time for higher mobility proteins to be replaced with proteins with a higher affinity for heparin. Thus, it is important to note that these *in vitro* experiments investigate the competitive binding of proteins with BMP-2 over longer periods, and they may not capture the kinetics of competitive protein binding that may occur *in vivo* immediately after implantation of the BMP-2-containing collagen sponge.

Mass spectrometry analysis of the serum proteins bound to heparin microparticles revealed a number of known heparin-binding proteins that display specific affinity for native heparin, including fibronectin ($K_D = 4 \, \mu M$),[48] thrombospondins ($K_D = 4$–$14 \, nM$),[49] and apolipoproteins ($K_D = 22$–$4000 \, nM$).[50,51] Other abundant proteins found in serum and known to nonspecifically bind to biomaterials implanted *in vivo*, such as albumin, globulins, and residual fibrinogen,[46] were also detected. Since the dissociation constant of heparin and BMP-2 is on a similar order of magnitude ($K_D = 20 \, nM$)[27] to that of fibronectin, thrombospondins, and apolipoproteins, these serum proteins may competitively bind to heparin and interfere with BMP-2 binding or increase its release in the bone defect environment. Others have also observed the binding of serum borne and endogenously added fibronectin

to heparin-containing materials *in vitro*.[52,53] Since fibronectin contains heparin-like growth factor-binding domains,[54,55] this ECM molecule may out-compete heparin for protein binding. Growth factor binding to fibronectin has been investigated extensively by using purified fibronectin fragments containing integrin and growth factor-binding domains, which have demonstrated enhanced binding of BMP-2 and other growth factors.[56,57]

Since the incorporation of more microparticles into the nanofiber mesh appeared to increase mesh delamination, linear heparin chains could be alternatively incorporated into the meshes to provide a more dispersed network of BMP-2 binding sites. Several studies have investigated the addition of varying amounts of heparin into PCL scaffolds by using electrospinning,[58] covalent immobilization,[59] or electrostatic assembly.[60] These methods could also be used to more evenly disperse heparin on the surfaces of the mesh tubes to facilitate more immediate contact between the immobilized heparin and diffusing BMP-2. Finally, since the promiscuity of heparin's binding sites may be responsible for the saturation of binding sites with serum components, the use of BMP-2-specific binding domains may circumvent some of the potential issues caused by serum adsorption and binding to microparticle-containing meshes. A more nuanced approach could include engineered protein-specific binding ligands[61] and derivatives of extracellular matrix molecules that possess a high affinity for specific proteins, such as fibronectin.[56,57] Ultimately, the incorporation of specific affinity molecules into biomaterials may improve the efficacy of growth factor sink approaches *in vivo*.

Conclusions

Overall, this study demonstrated the development of a hybrid nanofiber mesh with the purpose of spatially localizing BMP-2 delivery within a segmental bone defect. Although significant research has focused on developing materials for growth factor delivery, our approach to spatially control local BMP-2 diffusion presents a novel strategy to address clinical concerns of supraphysiological growth factor dose exposure. However, the mismatch between *in vitro* and *in vivo* results observed in this study highlights an important caveat in developing biomaterials for *in vivo* applications. Although growth factor binding and release performed *in vitro* provides valuable information about a biomaterial's ability to function as a delivery vehicle, in our study, it did not recapitulate the *in vivo* injury environment, and it led to an overestimation of the material's growth factor-binding capacity and an underestimation of its growth factor release *in vivo*. Our investigation revealed that the presence of serum components can significantly impact growth factor binding and release *in vitro*, suggesting that competitive protein binding *in vivo* may similarly hinder the ability of affinity-based biomaterials to modulate growth factor delivery. Thus, the results of this study may provide insights into the development and evaluation of other heparin-based protein delivery systems.

Acknowledgments

Disclosure Statement

No competing financial interests exist.

References

1. Mehta, M., Schmidt-Bleek, K., Duda, G.N., and Mooney, D.J. Biomaterial delivery of morphogens to mimic the natural healing cascade in bone. Adv Drug Deliv Rev **64,** 1257, 2012.

2. Urist, M.R., Mikulski, A., and Lietze, A. Solubilized and insolubilized bone morphogenetic protein. Proc Natl Acad Sci U S A **76,** 1828, 1979.

3. Wozney, J.M., Rosen, V., Celeste, A.J., Mitsock, L.M., Whitters, M.J., Kriz, R.W., Hewick, R.M., and Wang, E.A. Novel regulators of bone formation: molecular clones and activities. Science **242,** 1528, 1988.

4. Sampath, T., Muthukumaran, N., and Reddi, A. Isolation of osteogenin, an extracellular matrix-associated, bone-inductive protein, by heparin affinity chromatography. Proc Natl Acad Sci U S A **84,** 7109, 1987.

5. Allen, A.B., Priddy, L.B., Li, M.-T.A., and Guldberg, R.E. Functional augmentation of naturally-derived materials for tissue regeneration. Ann Biomed Eng **43,** 555, 2015.

6. Burkus, J.K., Gornet, M.F., Dickman, C.A., and Zdeblick, T.A. Anterior lumbar interbody fusion using rhBMP-2 with tapered interbody cages. J Spinal Disord Tech **15,** 337, 2002.

7. Burkus, J.K., Heim, S.E., Gornet, M.F., and Zdeblick, T.A. Is INFUSE bone graft superior to autograft bone? An integrated analysis of clinical trials using the LT-CAGE lumbar tapered fusion device, J Spinal Disord Tech **16,** 113, 2003.

8. Boden, S.D., Kang, J., Sandhu, H., and Heller, J.G. Use of recombinant human bone morphogenetic protein-2 to achieve posterolateral lumbar spine fusion in humans: a prospective, randomized clinical pilot trial. Spine **27,** 2662, 2002.

9. Govender, S., Csimma, C., Genant, H.K., Valentin-Opran, A,, Amit, Y., Arbel, R., Aro, H., Atar, D., Bishay, M., and Börner, M.G. Recombinant human bone morphogenetic protein-2 for treatment of open tibial fractures a prospective, controlled, randomized study of four hundred and fifty patients. J Bone Joint Surg **84,** 2123, 2002.

10. Boyne, P.J., Lilly, L.C., Marx, R.E., Moy, P.K., Nevins, M., Spagnoli, D.B., and Triplett, R.G. De novo bone induction by recombinant human bone morphogenetic protein-2 (rhBMP-2) in maxillary sinus floor augmentation. J Oral Maxillofac Surg **63,** 1693, 2005.

11. Chen, N.F., Smith, Z.A., Stiner, E., Armin, S., Sheikh, H., and Khoo, L.T. Symptomatic ectopic bone formation after off-label use of recombinant human bone morphogenetic protein-2 in transforaminal lumbar interbody fusion. J Neurosurg Spine **12,** 40, 2010.

12. Carragee, E.J., Hurwitz, E.L., and Weiner, B.K. A critical review of recombinant human bone morphogenetic protein-2 trials in spinal surgery: emerging safety concerns and lessons learned. Spine J **11,** 471, 2011.

13. Shields, L.B., Raque, G.H., Glassman, S.D., Campbell, M., Vitaz, T., Harpring, J., and Shields, C.B. Adverse effects associated with high-dose recombinant human bone morphogenetic protein-2 use in anterior cervical spine fusion. Spine **31,** 542, 2006.

14. Smucker, J.D., Rhee, J.M., Singh, K., Yoon, S.T., and Heller, J.G. Increased swelling complications associated with off-label usage of rhBMP-2 in the anterior cervical spine. Spine **31,** 2813, 2006.

15. Wong, D.A., Kumar, A., Jatana, S., Ghiselli, G., and Wong, K. Neurologic impairment from ectopic bone in the lumbar canal: a potential complication of off-label PLIF/TLIF use of bone morphogenetic protein-2 (BMP-2). Spine J **8,** 1011, 2008.

16. Friess, W., Uludag, H., Foskett, S., Biron, R., and Sargeant, C. Characterization of absorbable collagen sponges as rhBMP-2 carriers. Int J Pharm **187,** 91, 1999.

17. Geiger, M., Li, R.H., and Friess, W. Collagen sponges for bone regeneration with rhBMP-2. Adv Drug Deliv Rev **55,** 1613, 2003.

18. Uludag, H., D'Augusta, D., Golden, J., Li, J., Timony, G., Riedel, R., and Wozney, J.M. Implantation of recombinant human bone morphogenetic proteins with biomaterial carriers: a correlation between protein pharmacokinetics and osteoinduction in the rat ectopic model. J Biomed Mater Res **50,** 227, 2000.

19. Uludag, H., D'Augusta, D., Palmer, R., Timony, G., and Wozney, J. Characterization of rhBMP-2 pharmacokinetics implanted with biomaterial carriers in the rat ectopic model. J Biomed Mater Res **46,** 193, 1999.

20. McKay, W.F., Peckham, S.M., and Badura, J.M. A comprehensive clinical review of recombinant human bone morphogenetic protein-2 (INFUSE® Bone Graft). Int Orthop **31,** 729, 2007.

21. Sciadini, M.F., and Johnson, K.D. Evaluation of recombinant human bone morphogenetic protein-2 as a bone-graft substitute in a canine segmental defect model. J Orthop Res **18,** 289, 2000.

22. Zara, J.N., Siu, R.K., Zhang, X., Shen, J., Ngo, R., Lee, M., Li, W., Chiang, M., Chung, J., Kwak, J., Wu, B.M., Ting, K., and Soo, C. High doses of bone morphogenetic protein 2 induce structurally abnormal bone and inflammation in vivo. Tissue Eng Part A **17,** 1389, 2011.

23. Krishnan, L., Priddy, L.B., Esancy, C., Klosterhoff, B.S., Stevens, H.Y., Tran, L., and Guldberg, R.E. Delivery vehicle effects on bone regeneration and heterotopic ossification induced by high dose BMP-2. Acta Biomater **49,** 101, 2017.

24. Miller, T., Goude, M.C., McDevitt, T.C., and Temenoff, J.S. Molecular engineering of glycosaminoglycan chemistry for biomolecule delivery. Acta Biomater **10,** 1705, 2014.

25. Lindahl, U., and Hook, M. Glycosaminoglycans and their binding to biological macromolecules. Annu Rev Biochem **47,** 385, 1978.

26. Capila, I., and Linhardt, R.J. Heparin–protein interactions. Angew Chem Int Ed Engl **41,** 390, 2002.

27. Ruppert, R., Hoffmann, E., and Sebald, W. Human bone morphogenetic protein 2 contains a heparin-binding site which modifies its biological activity. Eur J Biochem **237,** 295, 1996.

28. Johnson, M.R., Boerckel, J.D., Dupont, K.M., and Guldberg, R.E. Functional restoration of critically sized segmental defects with bone morphogenetic protein-2 and heparin treatment. Clin Orthop Relat Res **469,** 3111, 2011.

29. Zhao, B., Katagiri, T., Toyoda, H., Takada, T., Yanai, T., Fukuda, T., Chung, U.-I. Koike, T., Takaoka, K., and Kamijo, R. Heparin potentiates the in vivo ectopic bone formation induced by bone morphogenetic protein-2. J Biol Chem **281,** 23246, 2006.

30. Abbah, S.A., Liu, J., Goh, J.C.H., and Wong, H.-K. Enhanced control of in vivo bone formation with surface functionalized alginate microbeads incorporating heparin and human bone morphogenetic protein-2. Tissue Eng Part A **19,** 350, 2012.

31. Kisiel, M., Klar, A.S., Ventura, M., Buijs, J., Mafina, M.-K., Cool, S.M., and Hilborn, J. Complexation and sequestration of BMP-2 from an ECM mimetic hyaluronan gel for improved bone formation. PLoS One **8,** e78551, 2013.

32. Yang, D.H., Lee, D.W., Kwon, Y.D., Kim, H.J., Chun, H.J., Jang, J.W., and Khang, G. Surface modification of titanium with hydroxyapatite-heparin-BMP-2 enhances the efficacy of bone formation and osseointegration in vitro and in vivo. J Tissue Eng Regen Med **9,** 1067, 2015.

33. Hu, T., Abbah, S.A., Wang, M., Toh, S.Y., Lam, R.W.M., Naidu, M., Bhakta, G., Cool, S.M., Bhakoo, K., and Li, J. Novel protamine-based polyelectrolyte carrier enhances low-dose rhBMP-2 in posterolateral spinal fusion. Spine **40,** 613, 2015.

34. Jeon, O., Song, S.J., Kang, S.-W., Putnam, A.J., and Kim, B.-S. Enhancement of ectopic bone formation by bone morphogenetic protein-2 released from a heparin-conjugated poly (L-lactic-co-glycolic acid) scaffold. Biomaterials **28,** 2763, 2007.

35. Hettiaratchi, M.H., Miller, T., Temenoff, J.S., Guldberg, R.E., and McDevitt, T.C. Heparin microparticle effects on presentation and bioactivity of bone morphogenetic protein-2. Biomaterials **35,** 7228, 2014.

36. Seto, S.P., Casas, M.E., and Temenoff, J.S. Differentiation of mesenchymal stem cells in heparin-containing hydrogels via coculture with osteoblasts. Cell Tissue Res **347,** 589, 2012.

37. Kolambkar, Y.M., Dupont, K.M., Boerckel, J.D., Huebsch, N., Mooney, D.J., Hutmacher, D.W., and Guldberg, R.E. An alginate-based hybrid system for growth factor delivery in the functional repair of large bone defects. Biomaterials **32,** 65, 2011.

38. Oest, M.E., Dupont, K.M., Kong, H.J., Mooney, D.J., and Guldberg, R.E. Quantitative assessment of scaffold and growth factor-mediated repair of critically sized bone defects. J Orthop Res **25,** 941, 2007.

39. Kolambkar, Y.M., Boerckel, J.D., Dupont, K.M., Bajin, M., Huebsch, N., Mooney, D.J., Hutmacher, D.W., and Guldberg, R.E. Spatiotemporal delivery of bone morphogenetic protein enhances functional repair of segmental bone defects. Bone **49,** 485, 2011.

40. Hayashi, M., and Yamada, K. Divalent cation modulation of fibronectin binding to heparin and to DNA. J Biol Chem **257,** 5263, 1982.

41. Hettiaratchi, M., Guldberg, R., and McDevitt, T. Biomaterial strategies for controlling stem cell fate via morphogen sequestration. J Mater Chem B **4,** 3464, 2016.

42. Lin, X. Functions of heparan sulfate proteoglycans in cell signaling during development. Development **131,** 6009, 2004.

43. Benoit, D.S., Collins, S.D., and Anseth, K.S. Multifunctional hydrogels that promote osteogenic human mesenchymal stem cell differentiation through stimulation and sequestering of bone morphogenic protein 2. Adv Funct Mater **17,** 2085, 2007.

44. Hudalla, G.A., Kouris, N.A., Koepsel, J.T., Ogle, B.M., and Murphy, W.L. Harnessing endogenous growth factor activity modulates stem cell behavior. Integr Biol **3,** 832, 2011.

45. Vroman, L., and Adams, A.L. Identification of rapid changes at plasma–solid interfaces. J Biomed Mater Res **3,** 43, 1969.

46. Wahlgren, M., and Arnebrant, T. Protein adsorption to solid surfaces. Trends Biotechnol **9,** 201, 1991.

47. Vroman, L., Adams, A., Fischer, G., and Munoz, P. Interaction of high molecular weight kininogen, factor XII, and fibrinogen in plasma at interfaces. Blood **55,** 156, 1980.

48. Ingham, K.C., Brew, S., and Atha, D.H. Interaction of heparin with fibronectin and isolated fibronectin domains. Biochem J **272,** 605, 1990.

49. Gupta, K., Gupta, P., Wild, R., Ramakrishnan, S., and Hebbel, R.P. Binding and displacement of vascular endothelial growth factor (VEGF) by thrombospondin: effect on human microvascular endothelial cell proliferation and angiogenesis. Angiogenesis **3,** 147, 1999.

50. Futamura, M., Dhanasekaran, P., Handa, T., Phillips, M.C., Lund-Katz, S., and Saito, H. Two-step mechanism of binding of apolipoprotein E to heparin: Implications for the kinetics of apolipoprotein E-heparan sulfate proteoglycan complex formation on cell surfaces. J Biol Chem **280,** 5414, 2005.

51. Gigli, M., Consonni, A., Ghiselli, G., Rizzo, V., Naggi, A., and Torri, G. Heparin binding to human plasma low-density lipoproteins: dependence on heparin sulfation degree and chain length. Biochemistry **31,** 5996, 1992.

52. Benoit, D.S., Durney, A.R., and Anseth, K.S. The effect of heparin-functionalized PEG hydrogels on three-dimensional human mesenchymal stem cell osteogenic differentiation. Biomaterials **28,** 66, 2007.

53. Benoit, D.S., and Anseth, K.S. Heparin functionalized PEG gels that modulate protein adsorption for hMSC adhesion and differentiation. Acta Biomater **1,** 461, 2005.

54. Wijelath, E.S., Rahman, S., Namekata, M., Murray, J., Nishimura, T., Mostafavi-Pour, Z., Patel, Y., Suda, Y., Humphries, M.J., and Sobel, M. Heparin-II domain of fibronectin is a vascular endothelial growth factor-binding domain: enhancement of VEGF biological activity by a singular growth factor/matrix protein synergism. Circ Res **99,** 853, 2006.

55. Rahman, S., Patel, Y., Murray, J., Patel, K.V., Sumathipala, R., Sobel, M., and Wijelath, E.S. Novel hepatocyte growth factor (HGF) binding domains on fibronectin and vitronectin coordinate a distinct and amplified Met-integrin induced signalling pathway in endothelial cells. BMC Cell Biol **6,** 8, 2005.

56. Martino, M.M., Tortelli, F., Mochizuki, M., Traub, S., Ben-David, D., Kuhn, G.A., Müller, R., Livne, E., Eming, S.A., and Hubbell, J.A. Engineering the growth factor microenvironment with fibronectin domains to promote wound and bone tissue healing. Sci Transl Med **3,** 100ra89, 2011.

57. Martino, M.M., Briquez, P.S., Maruyama, K., and Hubbell, J.A. Extracellular matrix-inspired growth factor delivery systems for bone regeneration. Adv Drug Deliv Rev **94,** 41, 2015.

58. Luong-Van, E., Grøndahl, L., Chua, K.N., Leong, K.W., Nurcombe, V., and Cool, S.M. Controlled release of heparin from poly(ε-caprolactone) electrospun fibers. Biomaterials **27,** 2042, 2006.

59. Singh, S., Wu, B.M., and Dunn, J.C.Y. The enhancement of VEGF-mediated angiogenesis by polycaprolactone scaffolds with surface cross-linked heparin. Biomaterials **32,** 2059, 2011.

60. Liu, L., Guo, S., Chang, J., Ning, C., Dong, C., and Yan, D. Surface modification of polycaprolactone membrane via layer-by-layer deposition for promoting blood compatibility. J Biomed Mater Res B Appl Biomater **87B,** 244, 2008.

61. Pakulska, M.M., Miersch, S., and Shoichet, M.S. Designer protein delivery: from natural to engineered affinity-controlled release systems. Science **351,** aac4750, 2016.

Address correspondence to:
Robert E. Guldberg, PhD
The Parker H. Petit Institute for Bioengineering
and Bioscience
Georgia Institute of Technology
315 Ferst Drive
Atlanta, GA 30332-0363

E-mail: robert.guldberg@me.gatech.edu

Laxminarayanan Krishnan, MBBS, PhD
The Parker H. Petit Institute for Bioengineering
and Bioscience
Georgia Institute of Technology
315 Ferst Drive
Atlanta, GA 30332-0363

E-mail: lkrishnan@gatech.edu